OMTO, Volume *24*

Supplemental information

Anti-CAIX BBζ CAR4/8 T cells exhibit superior efficacy in a ccRCC mouse model

Yufei Wang, Alicia Buck, Marion Grimaud, Aedin C. Culhane, Sreekumar Kodangattil, Cecile Razimbaud, Dennis M. Bonal, Quang-De Nguyen, Zhu Zhu, Kevin Wei, Madison L. O'Donnell, Ying Huang, Sabina Signoretti, Toni K. Choueiri, Gordon J. Freeman, Quan Zhu, and Wayne A. Marasco

Supplementary Materials

Supplemental Figures

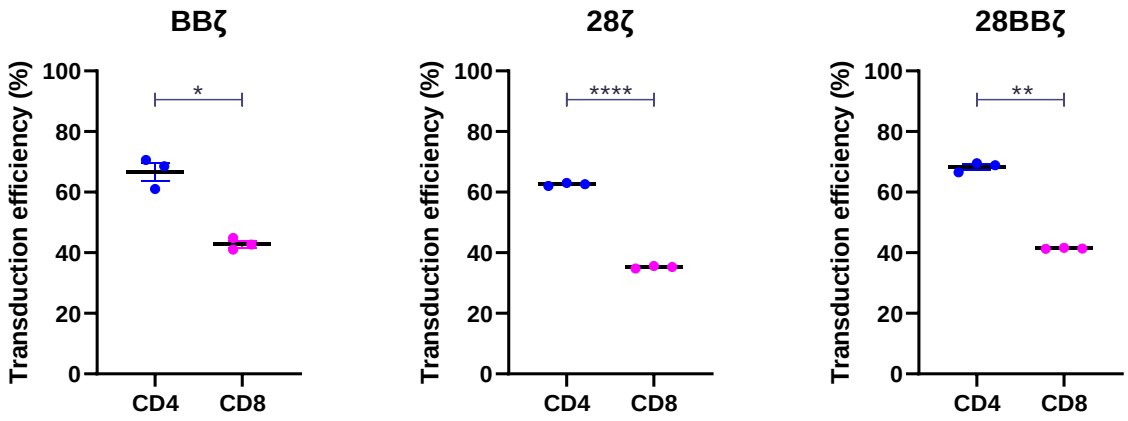

Supplementary Figure 1. Transduction efficiency of CAR-T. Transduction efficiency of CD4 (blue) and CD8 (pink) anti-CAIX BBζ, 28ζ, and 28BBζ CAR-T cells. ZsGreen expressing cells were quantified via flow cytometry and ZsGreen positivity was used to calculate transduction efficiency. *P* values are defined by unpaired two-tailed t-tests (∗p < 0.05; ∗∗p < 0.01; ∗∗∗p < 0.001; and ∗∗∗∗p < 0.0001).

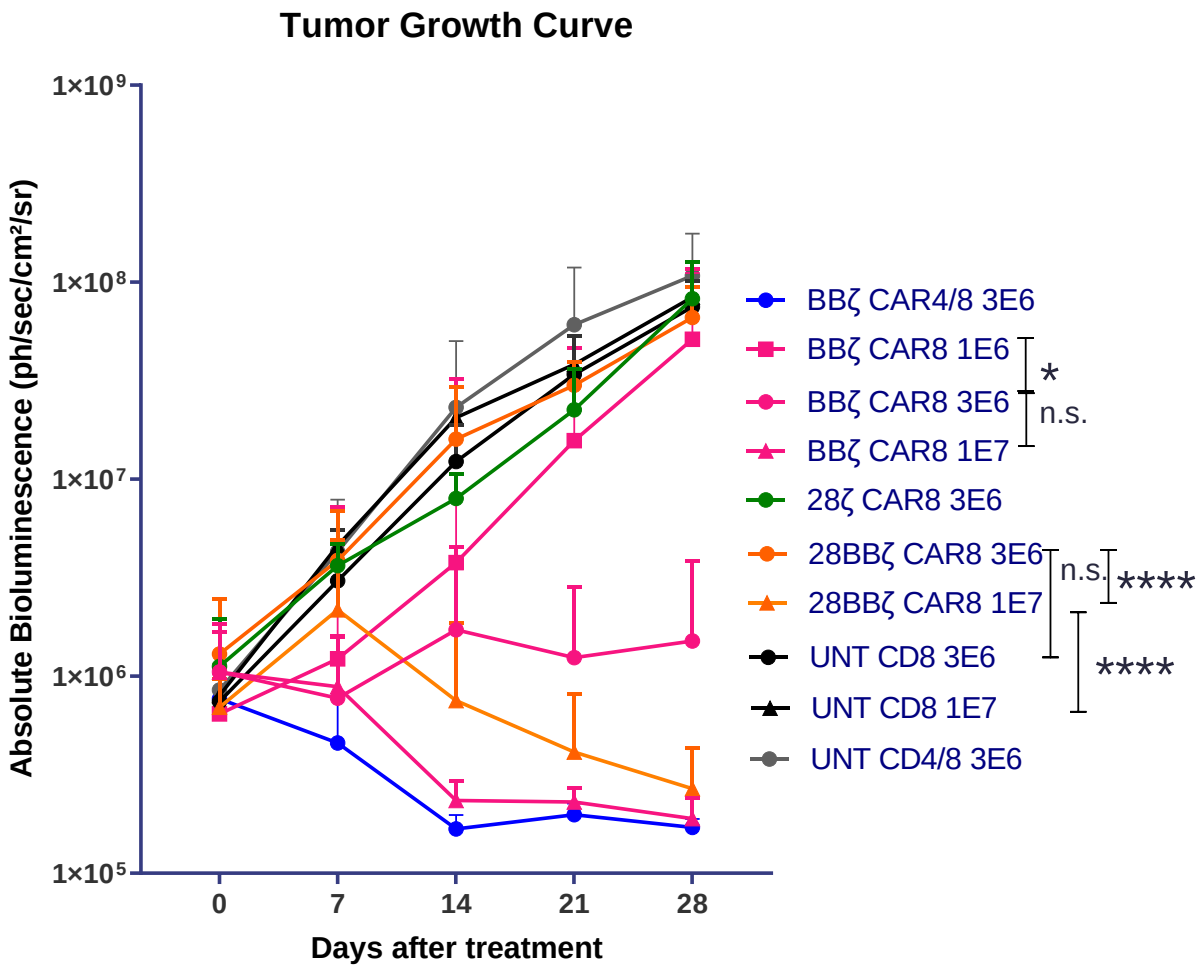

Supplementary Figure 2. Tumor growth curve of mice treated with 1 million cells of anti-CAIX BBζ CAR8, 3 million cells of BBζ CAR8, 28ζ CAR8, 28BBζ CAR8, BBζ CAR4/8, UNT CD8 and CD4/8 cells, 10 million cells of BBζ CAR8, 28BBζ CAR8, and UNT CD8. BLI was performed on Day 0, 7, 14, 21 and 28 after CAR-T infusion. *P* values are defined by ANOVA (∗p < 0.05; ∗∗p < 0.01; ∗∗∗p < 0.001; and ∗∗∗∗p < 0.0001).

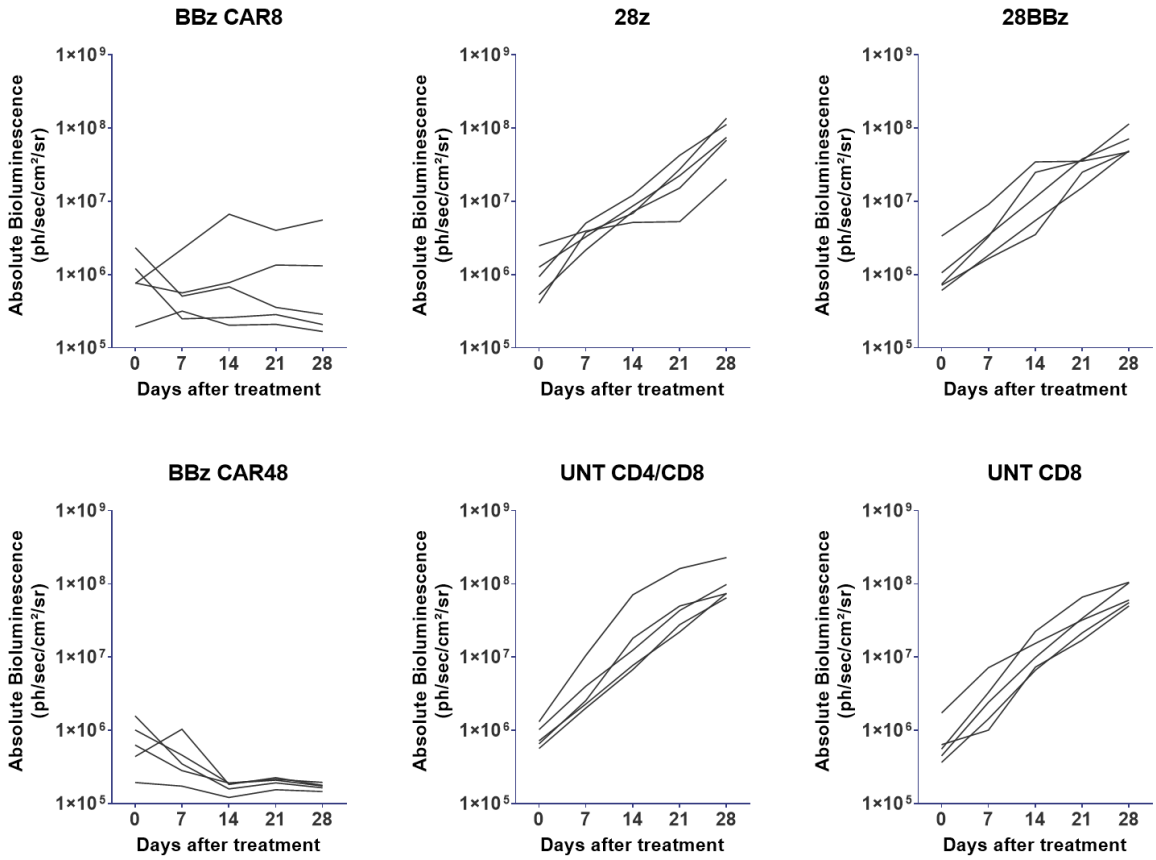

Supplementary Figure 3. Tumor growth curve of each individual mouse treated with anti-CAIX BBζ, 28ζ, 28BBζ, BBζ CAR4/8, CD8 and CD48 UNT cells. BLI was performed on Day 0, 7, 14, 21 and 28 after CAR-T infusion.

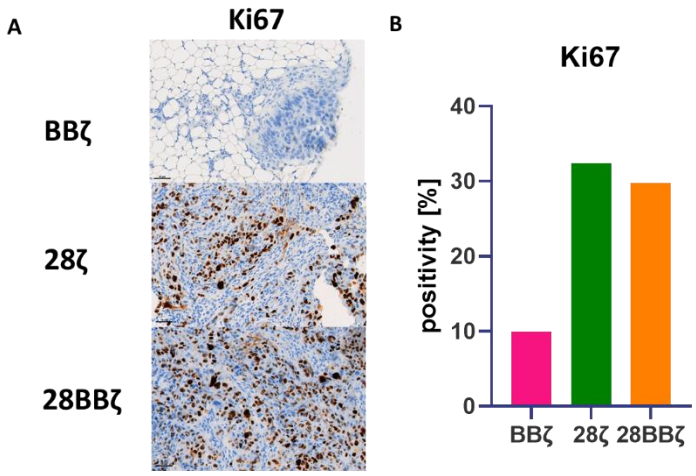

Supplementary Figure 4. IHC analysis of tumors treated with CAR-T cells. (A) Images of Ki67 staining on tumors treated with BBζ CAR8, 28ζ CAR8 and 28BBζ CAR8 cells (50x). (B) Quantification of Ki67+ tumor cells in tumors treated with BBζ CAR8 (pink), 28ζ CAR8 (green) and 28BBζ CAR8 (orange) cells.

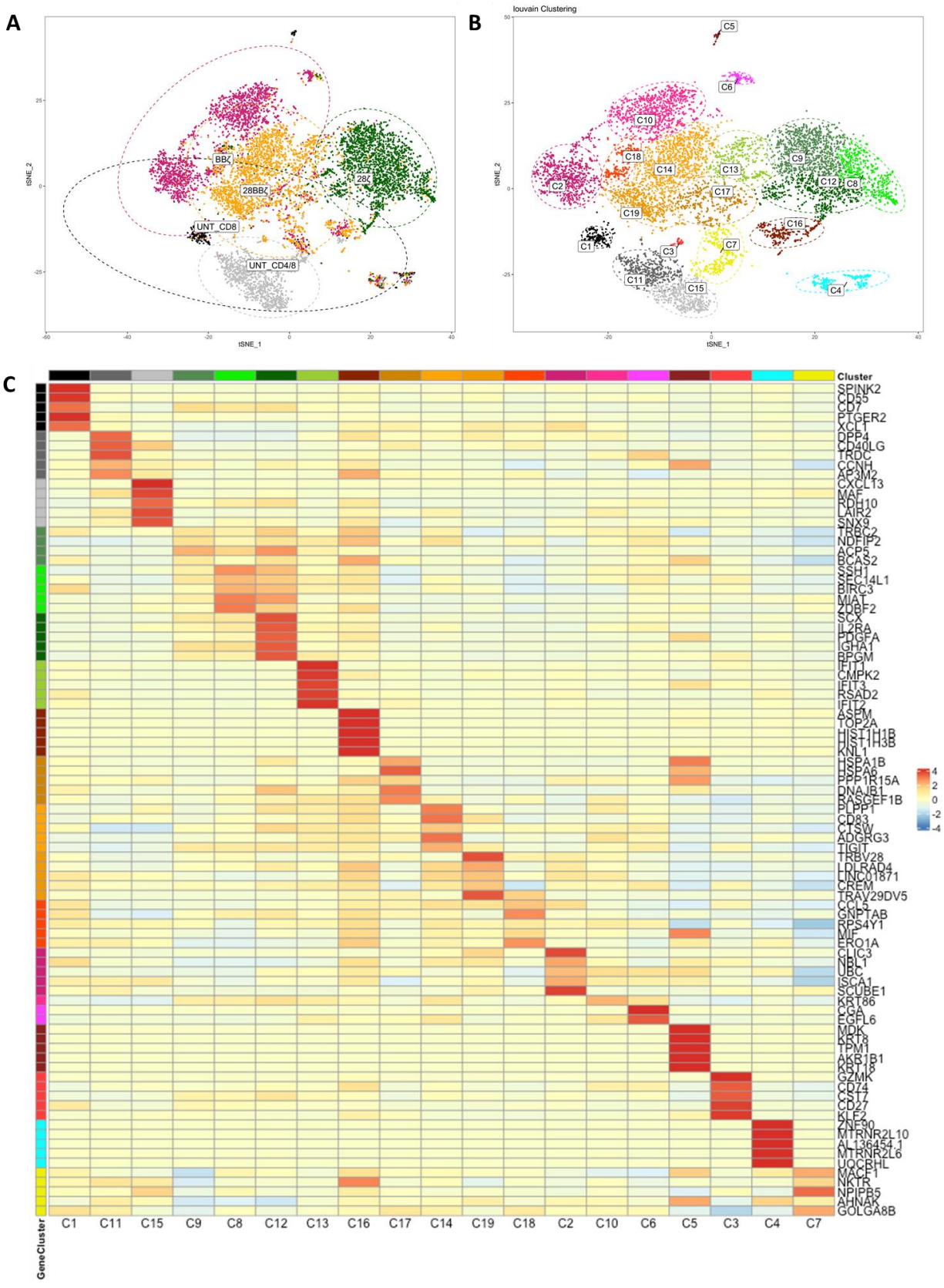
A
BBζ
28BBζ
28ζ
UNT_CD8
UNT_CD4/8
tSNE_1
tSNE_2
B
louvain Clustering
C5
C6
C10
C18
C14
C13
C9
C2
C17
C12
C8
C19
C16
C1
C3
C7
C11
C15
C4
C
Cluster
SPINK2
CD55
CD7
PTGER2
XCL1
DPP4
CD40LG
TRDC
CCNH
AP3M2
CXCL13
MAF
RDH10
LAIR2
SNX9
TRBC2
NDFIP2
ACP5
BCAS2
SSH1
SEC14L1
BIRC3
MIAT
ZDBF2
SOX4
IL2RA
PDGFA
IGHA1
RPGM
IFIT1
CMPK2
IFIT3
RSAD2
IFIT2
ASPM
TOP2A
HIST1H1B
HIST1H3B
KNL1
HSPA1B
HSPA6
PPP1R15A
DNAJB1
RASGEF1B
PLPP1
CD83
CTSW
ADGRG3
TIGIT
TRBV28
LDLRAD4
LINC01871
CREM
TRAV29DV5
CCL3
GNPTAB
RPS4Y1
MIF
ERO1A
CLIC3
NBL1
UBC
ISCA1
SCUBE1
KRT86
CGA
EGFL6
MDK
KRT8
TPM1
AKR1B1
KRT18
GZMK
CD74
CST7
CD27
KLF2
ZNF90
MTRNR2L10
AL136454.1
MTRNR2L6
UQCRHL
MACF1
NKTR
NPIPB5
AHNAK
GOLGA8B
4
2
0
-2
-4
Gene Cluster
C1
C11
C15
C9
C8
C12
C13
C16
C17
C14
C19
C18
C2
C10
C6
C5
C3
C4
C7

Supplementary Figure 5. Transcriptional signatures of tumor infiltrating T cells. (A) tSNE plot of tumor infiltrating T cells, colored by hashtag/ treatment group. This is same as Figure 4A and is shown here to have a better version when compare with panel B. (B) tSNE plot of tumor infiltrating T cells, colored by cluster assigned by Louvain clustering. 19 clusters were observed. (C) Top 5 differential expression genes ranked by *P* value from each cluster. The color bars on the top and side here reflect the color in the t-SNE plot.

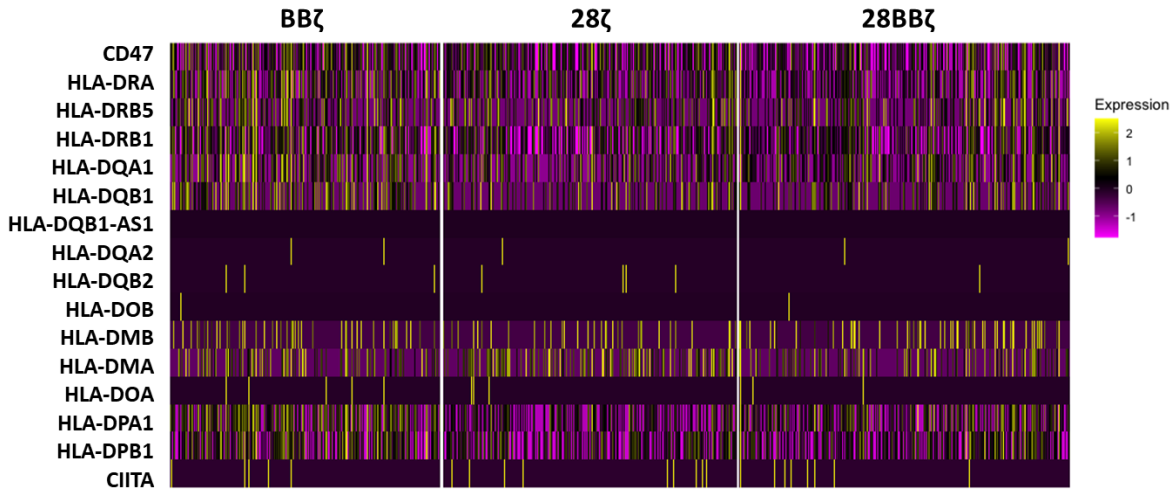

Supplementary Figure 6. Heatmap of MHC II genes in BBζ CAR8, 28ζ CAR8, 28BB CAR8. Sixteen MHC II genes, CD74, HLA-DRA, HLA-DRB5, HLA-DRB1, HLA-DQA1, HLA-DQB1, HLA-DQB1-AS1, HLA-DQA2, HLA-DQB2, HLA-DOB, HLA-DMB, HLA-DMA, HLA-DOA, HLA-DPA1, HLA-DPB1, and CIITA were shown in the heatmap. Seven low expression genes HLA-DQB1-AS1, HLA-DQA2, HLA-DQB2, HLA-DOB, HLA-DMB, HLA-DOA, CIITA were removed in **Figure 5. C and D**.

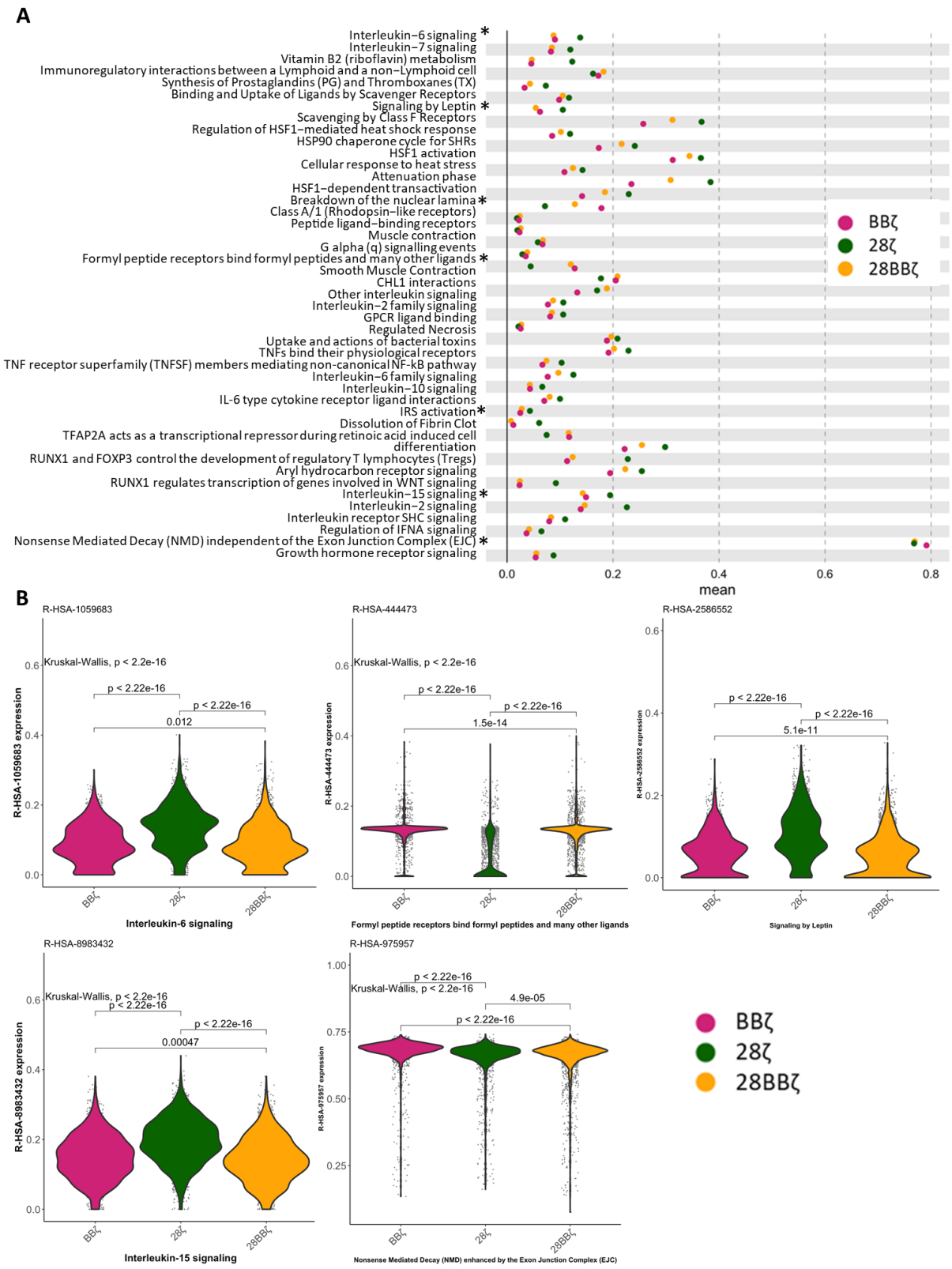
A
Interleukin−6 signaling *
Interleukin−7 signaling
Vitamin B2 (riboflavin) metabolism
Immunoregulatory interactions between a Lymphoid and a non−Lymphoid cell
Synthesis of Prostaglandins (PG) and Thromboxanes (TX)
Binding and Uptake of Ligands by Scavenger Receptors
Signaling by Leptin *
Scavenging by Class F Receptors
Regulation of HSF1−mediated heat shock response
HSP90 chaperone cycle for SHRs
HSF1 activation
Cellular response to heat stress
Attenuation phase
HSF1−dependent transactivation
Breakdown of the nuclear lamina *
Class A/1 (Rhodopsin−like receptors)
Peptide ligand−binding receptors
Muscle contraction
G alpha (q) signalling events
Formyl peptide receptors bind formyl peptides and many other ligands *
Smooth Muscle Contraction
CHL1 interactions
Other interleukin signaling
Interleukin−2 family signaling
GPCR ligand binding
Regulated Necrosis
Uptake and actions of bacterial toxins
TNFs bind their physiological receptors
TNF receptor superfamily (TNFSF) members mediating non−canonical NF−kB pathway
Interleukin−6 family signaling
Interleukin−10 signaling
IL−6 type cytokine receptor ligand interactions
IRS activation *
Dissolution of Fibrin Clot
TFAP2A acts as a transcriptional repressor during retinoic acid induced cell differentiation
RUNX1 and FOXP3 control the development of regulatory T lymphocytes (Tregs)
Aryl hydrocarbon receptor signaling
RUNX1 regulates transcription of genes involved in WNT signaling
Interleukin−15 signaling *
Interleukin−2 signaling
Interleukin receptor SHC signaling
Regulation of IFNA signaling
Nonsense Mediated Decay (NMD) independent of the Exon Junction Complex (EJC) *
Growth hormone receptor signaling
0.0
0.2
0.4
0.6
0.8
mean
BBζ
28ζ
28BBζ
B
R-HSA-1059683
Kruskal-Wallis, p < 2.2e-16
p < 2.22e-16
p < 2.22e-16
0.012
R-HSA-1059683 expression
Interleukin-6 signaling
R-HSA-444473
Kruskal-Wallis, p < 2.2e-16
p < 2.22e-16
p < 2.22e-16
1.5e-14
R-HSA-444473 expression
Formyl peptide receptors bind formyl peptides and many other ligands
R-HSA-2586552
p < 2.22e-16
p < 2.22e-16
5.1e-11
R-HSA-2586552 expression
Signaling by Leptin
R-HSA-8983432
Kruskal-Wallis, p < 2.2e-16
p < 2.22e-16
p < 2.22e-16
0.00047
R-HSA-8983432 expression
Interleukin-15 signaling
R-HSA-975957
p < 2.22e-16
Kruskal-Wallis, p < 2.2e-16
4.9e-05
p < 2.22e-16
R-HSA-975957 expression
Nonsense Mediated Decay (NMD) enhanced by the Exon Junction Complex (EJC)
BBζ
28ζ
28BBζ

Supplementary Figure 7. Pathway analysis of tumor infiltrating BBζ, 28ζ, and 28BBζ CAR-T cells. (A) 44 pathways ranked by Reactome ID. See **Table S4** for all *P* value results and **Table S5** for all FDR results. 44 pathways were selected using *P* value <0.001 and PairwiseWilcox statistic >0.7 in each pairwise comparison. AUC values of BBζ CAR8 (pink), 28ζ CAR8 (green), 28BBζ CAR8 (orange) in each pathway were shown in the plot. In seven pathways labeled with *, the AUC value of BBζ has a significant difference ($p<0.05$) compared to the value of 28BBζ. **(B) Five pathways with significant difference in comparison of BBζ and 28BBζ.** AUC values of BBζ CAR8 (pink), 28ζ CAR8 (green), 28BBζ CAR8 (orange) in each pathway (Interleukin-6 signaling, Formyl peptide receptors bind formyl peptides and many other ligands, Signaling by Leptin, Interleukin-15 signaling, and Nonsense Mediated Decay (NMD) independent of the Exon Junction Complex (EJC)) and corresponding *P* values of each pair comparison were shown in the plot.

Supplemental Tables

See Excel files online for full Supplemental Tables.